2026 IEEE/SICE International Symposium on System Integration (SII)
January 11-14, 2026. Cancún, México

Optimal Design of Passive Link Systems and Sensor Fusion for Precise Position Measurement of Robot End-Effector

Morito Sato[1], Atsushi Takata[1] and Masafumi Okada[1]

Abstract— **Many industrial robots utilize feedback control to perform precise tasks such as welding. The trajectory tracking performance of feedback control critically depends on the accuracy of sensor information, which often suffers from link deflection and homing error of the joint displacement sensors. To address these problems, this paper introduces lightweight and highly rigid passive link systems (PL) for acquiring measurement information with reduced deflection effects. To optimally integrate these redundant measurements, a sensor fusion method is developed, based on the resolution ellipsoid, to achieve precise estimation of the end-effector position. An optimal design methodology for the PL is also proposed, and the effectiveness of both proposals is validated experimentally. Moreover, to address biases observed in the experimental data relative to the true values, we propose a bias removal method based on Recursive Least Squares (RLS). We demonstrate through experimental data that this method enables precise position measurement of the end-effector.**

I. INTRODUCTION

In today's manufacturing, precise robot control is essential for producing high-quality products in large quantities. Particularly in welding processes, robots are required to perform weaving motions while precisely maintaining the vertical distance to the welded piece. Weaving is an essential robotic welding technique that enhances weld strength by increasing the weld bead width and volume through the periodic oscillation of the welding torch. The performance of arc sensing [1][2], which is central to automating this process, is significantly affected by the accuracy of the welded piece's vertical position, thereby influencing the final weld quality.

Achieving precise weaving motions requires the precise measurement of the end-effector position for feedback control. While the robot's end-effector position is kinematically determined from measured joint angles, its accuracy is primarily degraded by two factors. The first is the limited resolution of the joint angle sensors, while the second is calculation error arising from noise. Although the former issue can be addressed by using high-resolution encoders, this solution incurs a significant increase in implementation cost. The latter calculation error is mainly attributed to link deflection, which is caused by the weight of motors and reduction gears at each joint, and inaccuracies in homing. Link deflection is primarily categorized into static and dynamic deflection. Static deflection is caused by factors such as the link's own weight and the load applied to the end-effector. On the other hand, dynamic deflection may occur due to the inertial forces of the links generated by large accelerations and the torques from the actuators. This homing error is not only magnified by the complexity of the linkage system, but it also represents an uncertainty that cannot be corrected when relying on a single measurement source from internal sensors.

Non-contact external sensors, such as infrared sensors [3]-[5] and cameras [6][7], are sometimes employed to measure the robot position. Although these sensors are expected to achieve precise measurements owing to their capability for direct measurement of the absolute position, their susceptibility to the heat, light, and spatter generated by the welding arc precludes their prolonged use in the immediate vicinity. Consequently, they must often be positioned further from the arc, which deteriorates their measurement accuracy. For this reason, this study focuses on encoder-based measurement for determining the end-effector position. Unlike non-contact external sensors, encoders offer the advantage of providing precise measurements that are robust to the harsh welding environment.

In encoder-based measurement, link deflection poses a significant problem. Although methods based on flexible arm models, which account for the dynamic characteristics of deflection in a rigid arm [8]-[10], have been proposed to compensate for this problem, many of which primarily aim at vibration suppression rather than trajectory control, where the reference trajectory changes over time. Furthermore, the equations of motion for a flexible arm are considerably more complex than those for a rigid arm, making it extremely difficult to solve the inverse dynamics problem [11].

To address these problems, this study utilizes lightweight and highly rigid passive link systems (PL) [12] to acquire measurement values with reduced deflection effects. These link systems achieve their light weight without motors and reduction gears. This paper proposes a method to obtain a precise end-effector position estimate by fusing the multiple measurements obtained from the welding robot and the PL. This fusion is based on maximum likelihood estimation (MLE), wherein the likelihood function is determined by probabilistically interpreting the resolution ellipsoid derived from the singular value decomposition of the quadratic formulation of each Jacobian matrix [13][14]. This MLE is expected to enable the acquisition of measurement values at a higher resolution than that of the original robot. Based on this approach, an optimal design for the PL is developed, and its effectiveness is experimentally verified on a planar 3-link manipulator to evaluate weaving motion, with the PL

[1]Morito Sato, Atsushi Takata and Masafumi Okada are with the Department of Mechanical Engineering, School of Engineering, Institute of Science Tokyo, 2-12-1 Ookayama, Meguroku, Tokyo 152-8550, Japan sato.m.br@m.titech.ac.jp

978-1-6654-5784-2/26/$31.00 ©2026 IEEE

attached as shown in Fig.1. Furthermore, since each recorded data point from experiments contains a bias relative to its true value, we propose a bias removal method based on Recursive Least Squares (RLS), and we demonstrate through experimental data that this method enables precise position measurement of the end-effector.

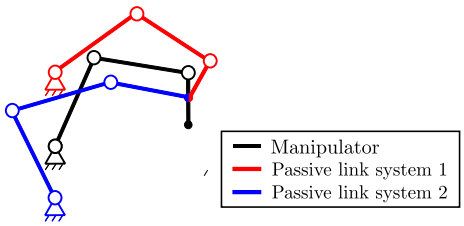

Fig. 1: Configuration of manipulator and PL.

II. Sensor fusion method

A. Evaluation of the end-effector resolution based on resolution ellipsoids

Sensor fusion for a manipulator and PL is performed based on the resolution ellipsoid. The resolution ellipsoid is determined by the link lengths and posture, and it represents the transformation of the angular resolution of each joint into the resolution for each direction of the end-effector position. By performing sensor fusion to minimize the resolution ellipsoid, an improvement in the measurement accuracy of the end-effector position can be expected.

Fig.2 shows the model of the manipulator and PL used in this study, where ℓ_j $(j = 1, 2, 3)$ denotes the link length, θ_j

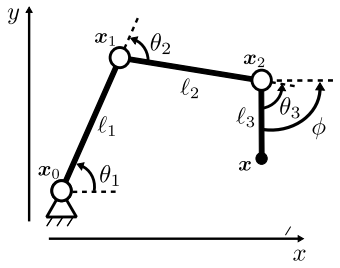

Fig. 2: Definition of variables for each parameter in the link system.

denotes the joint angle, $\boldsymbol{x}_j$ $(j = 0, 1, 2)$ denotes the joint position, $\boldsymbol{x}$ denotes the end-effector position, and ϕ denotes the posture angle respectively. The relationship between small deviation of the end-effector position (x, y) and joint angles $(\theta_1, \theta_2, \theta_3)$ can be expressed using the Jacobian matrix J as;

$$\Delta \boldsymbol{x} = J \Delta \boldsymbol{\theta}, \quad \boldsymbol{x} = \begin{bmatrix} x \\ y \end{bmatrix}, \quad \boldsymbol{\theta} = \begin{bmatrix} \theta_1 \\ \theta_2 \\ \theta_3 \end{bmatrix} \tag{1}$$

where the Jacobian matrix J is defined as:

$$J = \frac{\partial \boldsymbol{x}}{\partial \boldsymbol{\theta}} \tag{2}$$

Since joint angles are measured by encoders, the small deviation $\Delta\boldsymbol{\theta}$ in Eq.(1) can be expressed as;

$$\Delta \boldsymbol{\theta} = R \Delta \boldsymbol{p}, \quad R = \mathrm{diag}(r_1, r_2, r_3), \quad \boldsymbol{p} = \begin{bmatrix} p_1 \\ p_2 \\ p_3 \end{bmatrix} \tag{3}$$

where r_i represents the resolution of the encoder attached to each joint, and p_i represents the number of pulses from the encoder. Substituting Eq.(3) into Eq.(1), we obtain:

$$\Delta \boldsymbol{x} = JR \Delta \boldsymbol{p} \tag{4}$$

Considering the deviation per unit pulse, given by $\|\Delta \boldsymbol{p}\| = 1$, Eq.(4) can be transformed into;

$$\Delta \boldsymbol{x}^T \Sigma^{-1} \Delta \boldsymbol{x} = 1, \quad \Sigma = JRR^T J^T \tag{5}$$

where it is assumed that Σ is non-singular. Eq.(5) represents a resolution ellipsoid, and its conceptual diagram is shown in Fig.3. Directions of the shorter main axis represent the

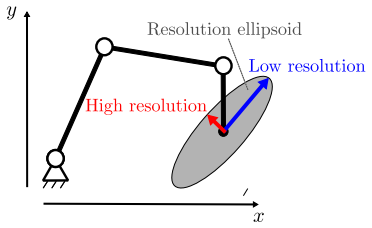

Fig. 3: Conceptual diagram of a resolution ellipsoid.

higher resolution, while the longer main axis represent the lower resolution.

B. Sensor fusion method based on autocovariance matrices of each link system

Since the contour lines of a multivariate normal distribution are represented by an ellipsoidal surface [15][16], the ellipsoid Σ_i derived in Section II-A can be interpreted as the autocovariance matrix in a multivariate normal distribution.

Let Σ_0, Σ_1, and Σ_2 be the autocovariance matrices of the manipulator, passive link system 1 (PL1), and passive link system 2 (PL2), respectively, in the xy-plane. Supposing the observed values are $\boldsymbol{x}_0$, $\boldsymbol{x}_1$, and $\boldsymbol{x}_2$, their respective probability density functions are given by;

$$f_0(\boldsymbol{x}) = \frac{1}{2\pi \sqrt{\left|\frac{\Sigma_0}{n}\right|}} \exp\left(-\frac{1}{2} \tilde{\boldsymbol{x}}_0^T \left(\frac{\Sigma_0}{n} \right)^{-1} \tilde{\boldsymbol{x}}_0 \right) \tag{6}$$

$$f_1(\boldsymbol{x}) = \frac{1}{2\pi \sqrt{|\Sigma_1|}} \exp\left(-\frac{1}{2} \tilde{\boldsymbol{x}}_1^T \Sigma_1^{-1} \tilde{\boldsymbol{x}}_1 \right) \tag{7}$$

$$f_2(\boldsymbol{x}) = \frac{1}{2\pi \sqrt{|\Sigma_2|}} \exp\left(-\frac{1}{2} \tilde{\boldsymbol{x}}_2^T \Sigma_2^{-1} \tilde{\boldsymbol{x}}_2 \right) \tag{8}$$

where

$$\tilde{\boldsymbol{x}}_i = \boldsymbol{x} - \boldsymbol{x}_i \quad (i = 0, 1, 2) \tag{9}$$

is defined and $n (0 < n < 1)$ is a weighting factor applied to the autocovariance matrix of the manipulator, reflecting its lower measurement accuracy due to link deflection compared to the PL. The likelihood function, which combines Eqs.(6), (7), and (8), is;

$$L(\boldsymbol{x}) = \prod_{i=0}^{2} f_i(\boldsymbol{x}) = f_0(\boldsymbol{x}) f_1(\boldsymbol{x}) f_2(\boldsymbol{x}) \tag{10}$$

and the MLE $\bar{\boldsymbol{x}}$ that maximizes this function is obtained from $\boldsymbol{x} = \bar{\boldsymbol{x}}$ satisfying $\partial L/\partial \boldsymbol{x} = 0$, and is expressed as;

$$\bar{\boldsymbol{x}} = \Sigma \left(\left(\frac{\Sigma_0}{n} \right)^{-1} \boldsymbol{x}_0 + \Sigma_1^{-1} \boldsymbol{x}_1 + \Sigma_2^{-1} \boldsymbol{x}_2 \right) \tag{11}$$

where

$$\Sigma = (n\Sigma_0^{-1} + \Sigma_1^{-1} + \Sigma_2^{-1})^{-1} \tag{12}$$

is defined. By performing sensor fusion using $\bar{\boldsymbol{x}}$ obtained from Eq.(11), a precise estimation of the end-effector position can be expected. Furthermore, the autocovariance around $\bar{\boldsymbol{x}}$ is represented by Σ in Eq.(12), which corresponds to the sum of the autocovariances of the manipulator and PL.

III. Optimization of PL

A. Design of the evaluation function

The design objective for the PL is to maximize the MLE from Eq.(11), which is achieved by minimizing the fused autocovariance matrix Σ given in Eq.(12). Specifically, we improve end-effector resolution by minimizing the Frobenius norm of the autocovariance Σ. The evaluation function for the design of the PL is defined as:

$$I(\boldsymbol{\eta}_1, \boldsymbol{\eta}_2) = I_1 + I_2 + I_3 + I_4 \tag{13}$$
$$I_1 = \|\alpha^2 \Sigma_r^{-1} - \Sigma^{-1}\|_F^2 \tag{14}$$
$$I_2 = -w_\alpha \|\alpha\|^2 \tag{15}$$
$$I_3 = w_0 \|0 - \boldsymbol{x}_0^1\| + w_1 \|\boldsymbol{x}_1^0 - \boldsymbol{x}_1^1\| + w_2 \|\boldsymbol{x}_2^0 - \boldsymbol{x}_2^1\| \tag{16}$$
$$I_4 = w_0 \|0 - \boldsymbol{x}_0^2\| + w_1 \|\boldsymbol{x}_1^0 - \boldsymbol{x}_1^2\| + w_2 \|\boldsymbol{x}_2^0 - \boldsymbol{x}_2^2\| \tag{17}$$

w represents the weight for each evaluation function, the superscript i in $\boldsymbol{x}_j^i$ distinguishes between the manipulator, PL1 and PL2, and j represents the joint position. The meaning of each term in the defined evaluation function is as follows:

- I_1 : This term is formulated to drive the fused autocovariance matrix Σ around $\bar{\boldsymbol{x}}$ toward a reference autocovariance matrix Σ_r. Σ_r is set according to the required accuracy.
- I_2 : This term aims to reduce the size of the Σ_r by maximizing the scaling factor α.
- I_3, I_4 : These terms bring the joints of the manipulator and PL closer to each other. By making the PL similar in shape to the manipulator, a sufficient range of motion is ensured without singular position.

The design variables $\boldsymbol{\eta}_1$ and $\boldsymbol{\eta}_2$ for the evaluation function in Eq.(13) are set as:

$$\boldsymbol{\eta}_1 = \begin{bmatrix} \ell_1^1 & \ell_2^1 & \ell_3^1 & \theta_1^1 & \theta_2^1 & \theta_3^1 & x_0^1 & y_0^1 & \phi^1 \end{bmatrix}^T \tag{18}$$
$$\boldsymbol{\eta}_2 = \begin{bmatrix} \ell_1^2 & \ell_2^2 & \ell_3^2 & \theta_1^2 & \theta_2^2 & \theta_3^2 & x_0^2 & y_0^2 & \phi^2 \end{bmatrix}^T \tag{19}$$

As for the constraints, in addition to matching the end-effector position of the manipulator and PL, the sum of the lengths of each PL is kept constant to prevent the PL from becoming excessively large or small.

B. Optimization results

The evaluation function in Eq.(13) is optimized using a gradient method subject to the defined constraints. The initial state of the optimization is shown in Fig.4(a), and the results are shown in Fig.4(b). The weights for the evaluation function, initial conditions for the optimization, and parameters are set as follows;

$$w_0 = 9, \quad w_1 = 0.55, \quad w_2 = 4, \quad w_\alpha = 40 \tag{20}$$
$$\alpha_{ini} = 3 \tag{21}$$
$$\boldsymbol{\ell}_{ini}^1 = \boldsymbol{\ell}_{ini}^2 = \begin{bmatrix} 0.5 & 0.45 & 0.3 \end{bmatrix}^T \tag{22}$$
$$\boldsymbol{x}_{0,ini}^1 = \begin{bmatrix} 0 & -0.02 \end{bmatrix}^T, \quad \boldsymbol{x}_{0,ini}^2 = \begin{bmatrix} 0 & 0.02 \end{bmatrix}^T \tag{23}$$
$$\Sigma_r = \mathrm{diag}(1, 1), \quad L = 1.15, \quad n = 0.5 \tag{24}$$

where L represents the sum of the passive link lengths. Comparing Fig.4(a) and Fig.4(b), it can be seen that the shape of PL has been optimized such that the reference ellipsoid (yellow line) becomes smaller, and simultaneously, the combined ellipsoid of the manipulator and PL (purple line) approaches the reference ellipsoid.

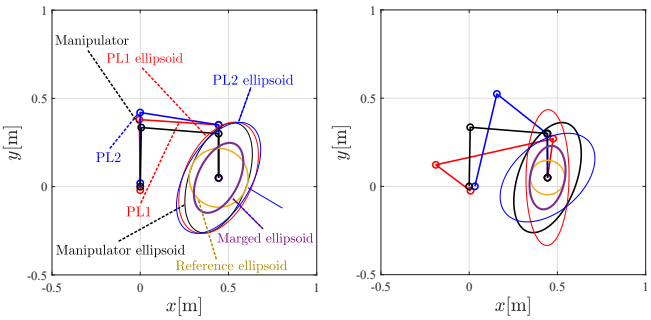

(a) Initial state. **(b)** Optimization result.

Fig. 4: Results of the optimization of PL to improve resolution in end-effector.

Table I shows the parameter values of the PL obtained from the optimization. Fig.5 illustrates the design and assembly based on these parameter values.

TABLE I: Parameter values of the manipulator and the PL obtained by optimization.

$\boldsymbol{\eta}$	Manipulator	PL1	PL2
ℓ_1 [mm]	335.0	246.0	538.0
ℓ_2 [mm]	439.5	681.0	364.0
ℓ_3 [mm]	250.0	223.0	248.0
x_0 [mm]	0.0	8.0	32.0
y_0 [mm]	0.0	−25.0	0.0
ϕ [rad]	−1.571	−1.751	−1.563

C. Evaluation of optimization results using resolution ellipsoid

Since the resolution ellipsoid represents the end-effector resolution in each direction, orthogonally projecting it onto the x-axis and y-axis allows for the determination of the end-effector resolution specific to the x and y directions, respectively. A conceptual diagram of this is shown in Fig.6.

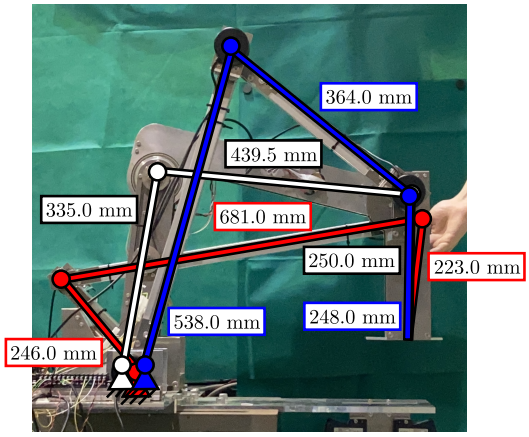

Fig. 5: Design of PL based on optimization.

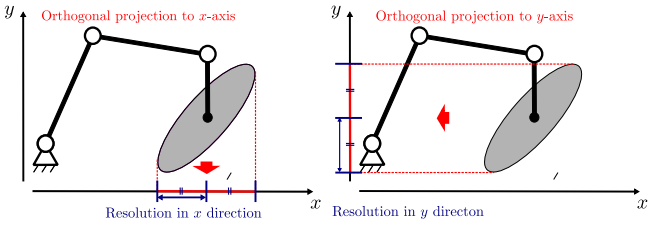

(a) Orthogonal projection to x-axis. **(b)** Orthogonal projection to y-axis.

Fig. 6: Orthogonal projection of a resolution ellipsoid onto each axis.

Assuming an encoder resolution of 9.0×10^{-4} deg for the manipulator and the PL, the autocovariance matrix of the manipulator Σ_0 and the autocovariance matrix Σ obtained from the optimization calculation are:

$$\Sigma_0 = \frac{2\pi}{4 \times 10^5} \begin{bmatrix} 0.146 & 0.103 \\ 0.103 & 0.389 \end{bmatrix} \tag{25}$$

$$\Sigma = \frac{2\pi}{4 \times 10^5} \begin{bmatrix} 0.0347 & 0.0314 \\ 0.0314 & 0.164 \end{bmatrix} \tag{26}$$

Based on these autocovariance matrices, the end-effector resolution for the x and y directions is presented in Table II. From Table II, calculating the ratios of the resolutions in

TABLE II: End-effector resolution for manipulator alone and PL with sensor fusion.

Resolution	Manipulator	Sensor fusion
x direction [mm]	6.01×10^{-3}	3.43×10^{-3}
y direction [mm]	9.83×10^{-3}	5.66×10^{-3}

the x and y directions for the manipulator and the optimized link system, R_x and R_y, yields:

$$R_x = \frac{3.43 \times 10^{-3}}{6.01 \times 10^{-3}} = 0.571 \tag{27}$$

$$R_y = \frac{5.66 \times 10^{-3}}{9.83 \times 10^{-3}} = 0.576 \tag{28}$$

This confirms that applying the link systems designed through optimization improves the end-effector resolution compared to the original manipulator.

IV. Measurement of Weaving Motion

A. Manipulator and weaving motion

Experiments are conducted using the link systems shown in Fig.5, which was designed and assembled in Section III. The manipulator is equipped with Harmonic Drive gears with a reduction ratio of 100 on each axis. It is driven by connecting DC motors to the input shafts via pulleys. DC motors of 90 W, 60 W, and 60 W are used from the base. Each motor axis has an incremental encoder with 1000 pulses per revolution. Since pulses are acquired with 4-multiplication, the resolution of each axis is $360 \text{ deg}/(1000 \text{ pulse} \times 4 \times 100) = 9.0 \times 10^{-4}$ deg. Each axis of the PL is equipped with an incremental encoder of 300,000 pulses per revolution. Similar to the manipulator, pulses are acquired with 4-multiplication, so the resolution of each axis is $360 \text{ deg}/(30 \times 10000 \text{ pulse} \times 4) = 3.0 \times 10^{-4}$ deg. The reference weaving motion is a periodic movement, and the reference trajectory is given by the end-effector position (x, y) and posture angle ϕ as follows:

$$\boldsymbol{w}^r(t) = \begin{bmatrix} x \\ y \\ \phi \end{bmatrix} = \begin{bmatrix} 0.444 + 0.020\sin(2\pi t) \\ 0.050 \\ -\dfrac{\pi}{2} \end{bmatrix} \tag{29}$$

This motion is illustrated in Fig.7 and is a fine motion relative to the size of the robot.

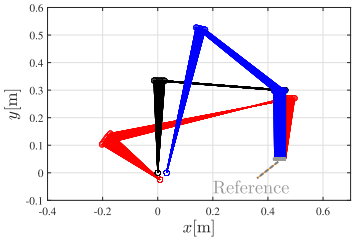

Fig. 7: Robot weaving motion.

B. Experimental results

When controlling the robot, feedforward input derived from inverse dynamics analysis and PID control are used. The PID gains for the end-effector coordinate system (horizontal direction, vertical direction, and posture angle, in order) are:

$$\begin{aligned} K_p &= \text{diag}(6000, 15000, 300) \\ K_d &= \text{diag}(80, 270, 20) \\ K_i &= \text{diag}(2500, 6000, 150) \end{aligned} \tag{30}$$

The gain in the end-effector vertical direction is set high to improve accuracy in the y direction. The PID controller utilizes only the encoder information from the manipulator. Furthermore, the end-effector position is measured by a laser displacement sensor (LK-G155) as an absolute position, which is assumed to be the true value. The measurement setup is illustrated in Fig.8. A major issue with this measurement method is that, when the end-effector is tilted, obtaining the y-coordinate requires the x-coordinate, which is itself difficult to measure accurately with an external sensor. To

address this issue, we utilize the fact that the installation distance between the two laser displacement sensors has sufficient margin for the weaving range, defining the range of existence of the end-effector's y-coordinate, Y_r, using the measured values L_1, L_2 from the laser displacement sensors as:

$$\min(L_1, L_2) \leq Y_r \leq \max(L_1, L_2) \tag{31}$$

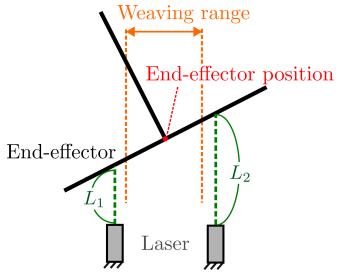

Fig. 8: Measurement method of the end-effector y-direction using laser displacement sensor.

The results of controlling the weaving motion shown in Fig.7 to the reference trajectory are presented in Fig.9. The black, red, and blue lines represent the end-effector positions calculated from the encoders of the manipulator, PL1, and PL2, respectively. The purple line represents the MLE calculated using Eq.(11), and the green region represents the range of existence of the true end-effector value, Y_r, as measured by the laser displacement sensors. The dashed lines represent the average of each measured value in the y-direction. From the experimental results, the following considerations are obtained:

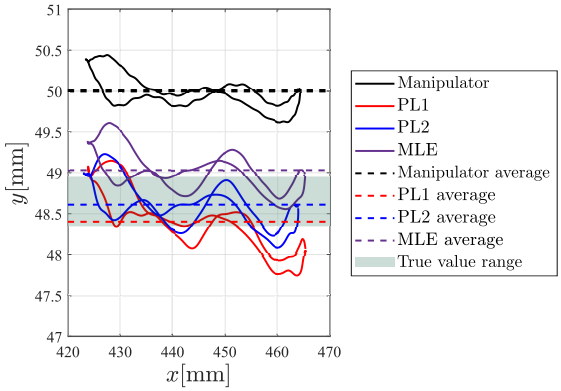

Fig. 9: Experimental results of each measured value and MLE.

1) While the PID feedback control, which utilizes only the manipulator's encoder measurements, ensures the end-effector trajectory closely follows the reference trajectory, it exhibits a significant bias relative to the true value range. This bias can be attributed to link deflection caused by the weight of motors and reduction gears at each joint, which introduces errors into the encoder-based position calculation.
2) The average value of PL2 is closer to the true value range compared to the manipulator. This indicates that the link does not deflect because motors and reduction gears are not attached, allowing accurate position measurement of the end-effector.
3) The average value of PL1 is closer to the true value range compared to the manipulator, but it has a constant bias. This is considered to be due to assembly errors and initial errors during the homing of the incremental encoders.
4) The average value of the MLE has a bias compared to the true value range. This suggests that since the manipulator and PL1 have biases, these biases remain even after sensor fusion.

These observations indicate that removing the bias from each measurement is essential for obtaining a MLE close to the true value, requiring a method for online bias compensation during the weaving motion.

C. Bias removal method using RLS

We compensate for the joint angle bias $\Delta\boldsymbol{\theta}_i$ of each measurement, assuming that the end-effector positions of the manipulator and PL are consistent. The joint angle biases that satisfy the consistency of each measured end-effector position are given by the relationship:

$$\begin{bmatrix} J_0 & -J_1 & 0 \\ J_0 & 0 & -J_2 \end{bmatrix} \begin{bmatrix} \Delta\boldsymbol{\theta}_0 \\ \Delta\boldsymbol{\theta}_1 \\ \Delta\boldsymbol{\theta}_2 \end{bmatrix} = \begin{bmatrix} \boldsymbol{x}_1 - \boldsymbol{x}_0 \\ \boldsymbol{x}_2 - \boldsymbol{x}_0 \end{bmatrix} \tag{32}$$

From this, we set Eq.(32) as;

$$\boldsymbol{J}\Delta\boldsymbol{\Theta} = \Delta\boldsymbol{X} \tag{33}$$

and use RLS to find the joint angle bias $\Delta\bar{\boldsymbol{\Theta}}_n$ that minimizes the evaluation function at time $t = n$;

$$J^{ev} = \sum_{t=1}^{n} (\Delta\boldsymbol{X}_t - \boldsymbol{J}_t\Delta\bar{\boldsymbol{\Theta}}_n)^T \lambda^{n-t} I (\Delta\boldsymbol{X}_t - \boldsymbol{J}_t\Delta\bar{\boldsymbol{\Theta}}_n)^T \tag{34}$$

where λ represents the forgetting factor. By calculating the bias-updated joint angles from the obtained joint angle bias $\Delta\bar{\boldsymbol{\theta}}_{i,n}$ as:

$$\bar{\boldsymbol{\theta}}_{i,n} = \boldsymbol{\theta}_{i,n} + \Delta\bar{\boldsymbol{\theta}}_{i,n} \tag{35}$$

We can obtain the bias-removed end-effector measurements $\bar{\boldsymbol{x}}_{i,n}$ and the MLE $\bar{\boldsymbol{x}}_n$.

D. Experimental results with bias removal

Fig.10 shows the results of bias removal based on RLS described in Section IV-C. Table III compares the average y-direction values from Fig.9 and Fig.10. The parameters for performing RLS are set as:

$$\lambda_i = 1 - 1 \times 10^{-6}, \quad P_0 = 1.5 \times 10^{-1} I \tag{36}$$

From the results in Table III, it was confirmed that by performing sequential bias removal, the average values for the manipulator and PL fall within the true value range, indicating that the bias has been successfully removed. This demonstrates that by combining information only from internal sensors (encoders), measurements equivalent to those from external sensors (laser displacement sensors) can be achieved.

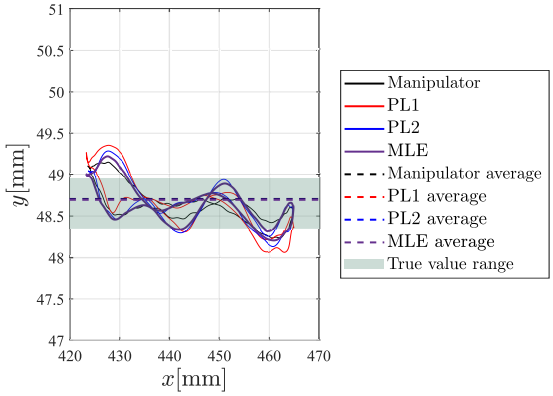

Fig. 10: Experimental results after bias removal.

TABLE III: Comparison of average y-direction values from Fig. 9 and Fig. 10.

	Before Removal [mm]	After Removal [mm]
Manipulator	50.00	48.70
PL1	48.40	48.70
PL2	48.61	48.70
MLE	49.03	48.70
True value range	$48.35 \sim 48.95$	$48.35 \sim 48.95$

V. Conclusion

In this study, we proposed a sensor fusion method for a manipulator and PL to obtain precise sensor measurements by attaching PL to the manipulator. Based on this, we performed optimization of the PL design and conducted experiments for precise position measurement of the end-effector. This paper is summarized as follows:

1) We proposed an evaluation method for end-effector resolution based on the resolution ellipsoid.
2) A sensor fusion method was developed based on MLE. This method constructs a likelihood function from the autocovariance matrices, which are derived from the respective resolution ellipsoid, to determine the most probable end-effector position.
3) Based on the proposed sensor fusion method, we optimized the shape of the PL to maximize the likelihood. We confirmed and experimentally demonstrated that the optimized PL improves end-effector resolution.
4) We proposed a bias removal method based on the RLS. By correcting experimental data based on this method, the biases in each measurement were compensated, confirming that precise position measurement of end-effector equivalent to that achieved with external sensors can be realized even when combining only internal sensors.

Acknowledgments

This research was supported by a joint research project with Kobe Steel, Ltd., titled “Research on Improving Weaving Motion Accuracy of Robots Based on Sensitivity Analysis of Model Parameters.”

References

[1] D. Baek, H. S. Moon, and S-H. Park, “Development of an automatic orbital welding system with robust weaving width control and a seam-tracking function for narrow gap”, The International Journal of Advanced Manufacturing Technology, Vol. 93, No. 4, pp. 1-11, 2017.

[2] C. Kang, Z. Liu, S. Chen, and X. Jiang, “Circular trajectory weaving welding control algorithm based on space transformation principle”, Journal of Manufacturing Processes, Vol.46, pp.328-336, 2019.

[3] Nagarajan, S., P. Banerjee, W. Chen, B. Chin, “Control of the Process Using Infrared Sensors”, IEEE Transaction on Robotics and Automation, Vol. 8, No. 1, pp. 86-93, 1992.

[4] H.C Wikle, S Kottilingam, R.H Zee and B.A Chin, “Infrared sensing techniques for penetration depth control of the submerged arc welding process”, Journal of Materials Processing Technology, Vol. 113(1-3), pp. 228-233, 2001.

[5] Haibo Fan, Nanda K Ravala, Howard C Wikle and Bryan A Chin, “Low-cost infrared sensing system for monitoring the welding process in the presence of plate inclination angle”, Journal of Materials Processing Technology, Vol. 140(1-3), pp. 668-675, 2003.

[6] L. H. Sharif, S. Yamane, Y. Hino, K. Eguchi, T. Kubota and K. Oshima, “Sensing and digital control of weld pool with visual welding robot”, 2000 26th Annual Conference of the IEEE Industrial Electronics Society. IECON 2000. 2000 IEEE International Conference on Industrial Electronics, Control and Instrumentation. 21st Century Technologies, Nagoya, Japan, Vol. 3, pp. 1521-1526, 2000.

[7] Zhang, Y, Kovacevic, R and Li, L, “Characterization and real-time measurement of geometrical appearance of the weld pool”, Int. J. Mach. Tools Manufact. Vol. 36, No. 7, pp. 799-816, 1996.

[8] W. J. Book, O. Maizza-neto, D. E. Whitney, “Feedback Control if Two Beam, Two Joint Systems With Distributed Flexibility”, Journal of Dynamic Systems, Measurement, and Control, Vol. 97, No. 4, pp. 424-431, 1975.

[9] W. He, Y. Ouyang, J. Hong, “Vibration Control of a Flexible Robotic Manipulator in the Presence of Input Deadzone”, IEEE Transactions on Industrial Informatics, Vol. 13, No. 1, pp. 48-59, 2017.

[10] A. Jnifene, W. Andrews, “Experimental study on active vibration control of a single-link flexible manipulator using tools of fuzzy logic and neural networks”, IEEE Transactions on Instrumentation and Measurement, Vol. 54, No. 3, pp. 1200-1208, 2005.

[11] A. A. Alqumsan, S. Khoo, and M. Norton, “Robust control of continuum robots using cosserat rod theory”, Mechanism Mach. Theory, Vol. 131, pp. 48–61, 2019.

[12] J. Hesselbach, C. Bier, I. Pietsch, N. Plitea, S. Büttgenbach, A. Wogersien, J. Güttler, “Passive-joint sensors for parallel robots”, Mechatronics, Vol. 15(1), pp. 43-65, 2005.

[13] S. Chiu, “Control of redundant manipulators for task compatibility,” Proceedings. 1987 IEEE International Conference on Robotics and Automation, Raleigh, NC, USA, pp. 1718-1724, 1987.

[14] P. Chiacchio, S. Chiaverini, L. Sciavicco, and B. Siciliano, “Global task space manipulability ellipsoids for multiple-arm systems”, IEEE Trans. Robot. Automat., Vol. 7, No. 5, pp. 678-685, Oct. 1991.

[15] M. Friendly, G. Monette, and J. Fox, “Elliptical insights: Understandingstatistical methods through elliptical geometry”, Stat. Sci., Vol. 28, No. 1, pp. 1-39, Feb. 2013.

[16] C.G Khatri, Rahul Mukerjee, “Characterization of normality within the class of elliptical contoured distributions”, Statistics & Probability Letters, Vol. 5(3), pp. 187-190, 1987.